Synthesis of Ag/Bi_2MoO_6 composite nanosheets for enhanced photocatalytic degradation of RhB solution

Z. X. Dai[a], L.Y. Zhang[b,c], C.L.Ruan[c], Z.Q.Yun[c], G.H. Zheng[c*]

[a]*Institutes of Physical Science and Information Technology, Anhui University, Hefei 230601, China*

[b]*Key Laboratory of Structure and Functional Regulation of Hybrid Materials (Anhui University), Ministry of Education, Hefei, 230601, China*

[c]*School of Physics and Materials Science, Anhui University, Hefei 230039, China*

[d]*School of Energy Materials and Chemical Engineering, Hefei University, Hefei 230601, China*

Visible-light-driven photocatalyst Ag/Bi_2MoO_6 was successfully synthesized via a facile hydrothermal route. Ag was uniformly dispersed on the surface of Bi_2MoO_6 nanosheets. The photocatalytic performance of Ag/Bi_2MoO_6 composites was evaluated by the degradation of Rhodamine B (RhB). The Ag/Bi_2MoO_6 nanocomposite exhibited a higher photocatalytic activity as compared to pure Bi_2MoO_6. Moreover, the 7wt% Ag-loaded Bi_2MoO_6 showed the optimal photocatalytic performance in the degradation of RhB. The photogenerated holes (h^+) and superoxide radical anions ($\bullet O^{2-}$) were found to be the primary reactive species in the degradation of RhB dye in aqueous solution.

(Received April 12, 2021; Accepted February 5, 2022)

Keywords: Bi_2MoO_6, Ag loading, Photocatalyst

1. Introduction

Bismuth-containing semiconductors, such as Bi_2MoO_6,[1] Bi_2O_3,[2] and BiOX[3] have been extensively investigated as efficient photocatalysts due to their good chemical stability and large response toward visible light.[4,5] In this regard, the two dimensional (2D) nanosheet array has attracted much attention because of two reasons. First, high orientation can provide uniform pathways for efficient charge transfer and separation. Second, high surface-to-volume ratios and open-edge geometry of the nanosheet array can improve the solar conversion efficiency. Among the Bi-based compounds, Bi_2MoO_6 with a narrow band gap (2.5-2.8eV) shows good photocatalytic activity in presence of visible light.[6,7] Moreover, Bi_2MoO_6 is characterized by alternative perovskite $(MoO_4)^{2+}$ slaps and stacking of $(Bi_2O_2)^{2+}$ layers, which facilitates effective separation of photoinduced electron-hole pairs, resulting in high photocatalytic activity.[8] However, it is thought that pure Bi_2MoO_6 photocatalysts have some drawbacks, including low efficiency in separating photogenerated electron-hole pairs, which limits its practical applications. In order to overcome

* Corresponding author: ghzheng@ahu.edu.cn

https://doi.org/10.15251/DJNB.2022.171.179

these drawbacks, some efforts have been made, such as rare earth elements doping,[9] morphology control,[10] loading metal or metal oxide to form heterostructures.[11,12]

Ag-loading on photocatalyst is a new approach to increase the separation rate of photogenerated electrons and holes and improve the photocatalytic efficiency.[13,14] For example, Zhou et al fabricated three transitional metals (Ag, Ni, and Co) loaded $BiVO_4$ particles using amorphous heteronuclear complexing method and reported that the photocatalysts exhibited significant photocatalytic efficiency in the degradation of methyl blue.[15] Using $AgNO_3$ as additive, Wang et al prepared $BiVO_4$:Ag composites, where Ag islands were formed on the surface of $BiVO_4$ to generate Ag:$BiVO_4$ heterostructure. As a result, the photocatalytic properties were enhanced largely.[16] The enhanced photocatalytic activity of Ag-based composites is generally attributed to the surface plasmon resonance (SPR) effect of the Ag nanoparticles on the surface of the composites.[17] When Ag nanoparticles contact with a charged semiconductor, it can harvest visible light more effectively through SPR effect to produce electrons on their surfaces, and these electrons transfer to the adjacent semiconductor through interface.[18] Such electron transfer greatly increases the separation rate of photogenerated electrons and holes and improves the photocatalytic efficiency for Ag-loading compounds.

In the present study, we report the synthesis of Ag/Bi_2MoO_6 composite photocatalyst via hydrothermal process. The as-prepared Ag/Bi_2MoO_6 composite photocatalyst exhibited visible light photocatalytic activity toward rhodamine B (RhB) degradation.

The results suggested that the large surface area of Bi_2MoO_6 nanosheets, large heterojunctions between Bi_2MoO_6 and Ag, and visible light absorption are helpful for the enhancement of the material's photocatalytic activity. The mechanism for the photocatalytic degradation of RhB over the Ag/Bi_2MoO_6 nanostructures has also been discussed.

2. Experimental

2.1. Materials synthesis

2.1.1. Synthesis of Bi_2MoO_6 Photocatalyst

Pure Bi_2MoO_6 sample was prepared via hydrothermal route. Stoichiometric amount of $Bi(NO_3)_3 \cdot 5H_2O$ was dissolved in ethylene glycol. $Na_2MoO_4 \cdot 2H_2O$ and NaOH were separately dissolved in deionized water by stirring for 30min using a magnetic stirrer. The NaOH solution was added to adjust the pH value to 7. A certain amount of sodium dodecyl sulfate (SDS) dissolved in deionized water was added drop wise to the above mixture under vigorous stirring for 30min. Next, the mixture was placed in a 1000 mL hastelloy autoclave (Parr 4577) and reacted at 160 ^oC for 12h. After the autoclave was cooled to room temperature naturally, the products were separated by centrifugation, washed sequentially with ethanol and deionized-water several times, and finally dried at 80 ^oC to obtain the Bi_2MoO_6 sample.

2.1.2. Synthesis of Ag/Bi_2MoO_6 Composite Photocatalyst

Ag nanoparticles were obtained via a modified method reported by Yang et al.[19] An amount of Bi_2MoO_6 were dissolved in ethylene glycol under magnetic stirring for 10min. Then, different amounts of $AgNO_3$ were added to the above mixture under vigorous agitation. The suspension was sonicated for 30min. The obtained suspension was then sealed in Teflon-lined

stainless autoclave and heated at 150 ^{o}C for 120min. After cooling to room temperature naturally, the product was washed several times with deionized water and ethanol followed by drying at 80 ^{o}C to obtain the final samples.

A flowchart for the synthesis of Ag loaded Bi_2MoO_6 composite photocatalyst has been presented in Figure 1(A). Additionally, the corresponding growth mechanism of Ag loaded Bi_2MoO_6 composite photocatalyst has been proposed in Figure 1(B).

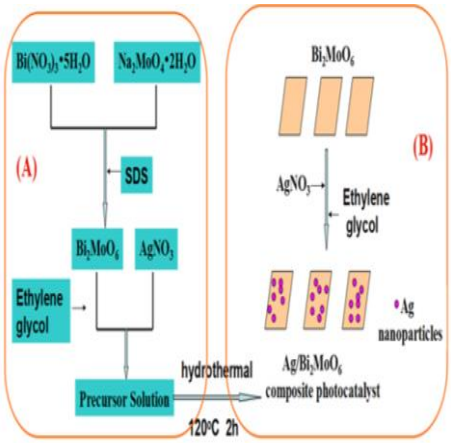

Fig. 1. (A) Flowchart for synthesis of Ag/Bi_2MoO_6 composite photocatalyst; (B) Growth mechanism of Ag/Bi_2MoO_6 composite photocatalyst.

2.2. Characterizations

The crystal structure of the product was characterized by XRD using an X-ray diffractometer (XRD dx-2000 SSC) with Cu Kα radiation (λ=1.5418Å) over a scanning range of 10-80º with a step of 0.02º. Using X-ray photoelectron spectroscopy (XPS, Elcalab 250 Xi, American), the valence states of ions were also tested. Surface morphologies and lattice fringes were observed through scanning electron microscopy (SEM, S-4800, Hitachi) and High resolution transmission electron microscopy (HRTEM, JEOL JEM-2100). Optical diffuse reflectance spectra were recorded on a Japan Shimazdu UV-3600 (Japan) using $BaSO_4$ as a reference.

2.3. Photocatalytic Reactions

The photocatalytic activities of Bi_2MoO_6 samples were evaluated by investigating the degradation of methyl blue under a 350W Xe lamp light. In each experimental, 200mg of the photocatalyst was added to 80mL of Rhodamine B (RhB) solution (10mg/L) in a test tube. Before illumination, the suspensions were magnetically stirred in the dark for 60min to ensure establishment of adsorption-desorption equilibrium between the photocatalysts and RhB. The solution under magnetic stirring was then exposed to Xe lamp light irradiation. At a given interval, the test tubes were sampled and then centrifuged to remove the photocatalyst particles.

3. Results and discussions

3.1. Structure and Phase Analysis

The crystal structures of Bi_2MoO_6 and Ag/Bi_2MoO_6 samples were examined by XRD, as shown in Figure 2. The diffraction peaks for all the samples were perfectly indexed as pure orthorhombic Bi_2MoO_6 phase which matched well with the standard card (JCPDS no. 21-0102). No Ag peaks were observed in the XRD pattern of Ag/Bi_2MoO_6 nanoparticles, which may be due to a very low amount of the Ag metal dispersed in the material.

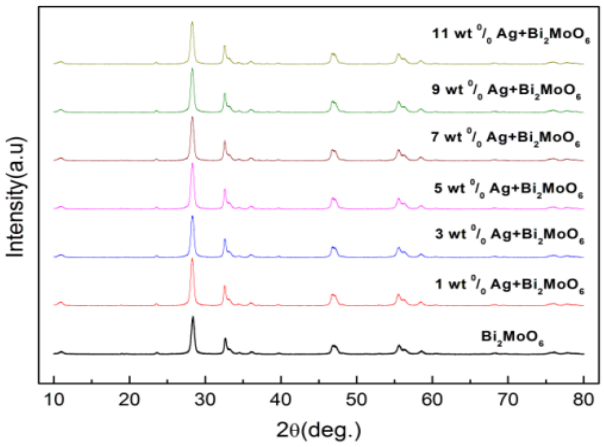

Fig. 2. XRD patterns of the as-synthesized 0 wt%, 1 wt%, 3 wt%, 5 wt%, 7 wt%, 9 wt%, and 11 wt% loaded Bi_2MoO_6 samples.

XPS measurement was employed to study the chemical composition and surface chemical state of the as-synthesized Ag/Bi_2MoO_6 composites. Figure 3 presents the wide scanning spectrum of 7wt%Ag loaded Bi_2MoO_6 and individual bands, respectively. The fully typical scanned spectrum of the Ag/Bi_2MoO_6 nanocomposites in the range from 0 to 1200eV is shown in Figure 3a, which clearly indicated the co-existence of Ag, Mo, Bi, and O. The obvious peaks corresponding to Bi5d, Bi5p, Bi4f, Bi4d, Bi4p, Mo3d, Mo3p, C1s, O1s and Ag3d could be detected, as shown in Figure 3(a). To further identify the chemical state of the energy element, high resolution XPS spectrum of 7wt%Ag loaded Bi_2MoO_6 was recorded and presented in Figure 3(b)-(d). The peaks centered at 164.4 eV and 159.1 eV were assigned to Bi $4f_{7/2}$ and Bi $4f_{5/2}$, indicating that the Bi species in our samples is in the form of Bi^{3+}.[20] The value of 235.6 and 232.4eV for Mo $3d_{5/2}$ and Mo $3d_{3/2}$ can be assigned to a Mo^{6+} oxidation state,[21] as presented in Fig 3(c). The peaks at 368.1 eV and 374.1eV were assigned as the Ag $3d_{5/2}$ and Ag $3d_{3/2}$ binding energy, respectively, as shown in Figure 3(d).[22]

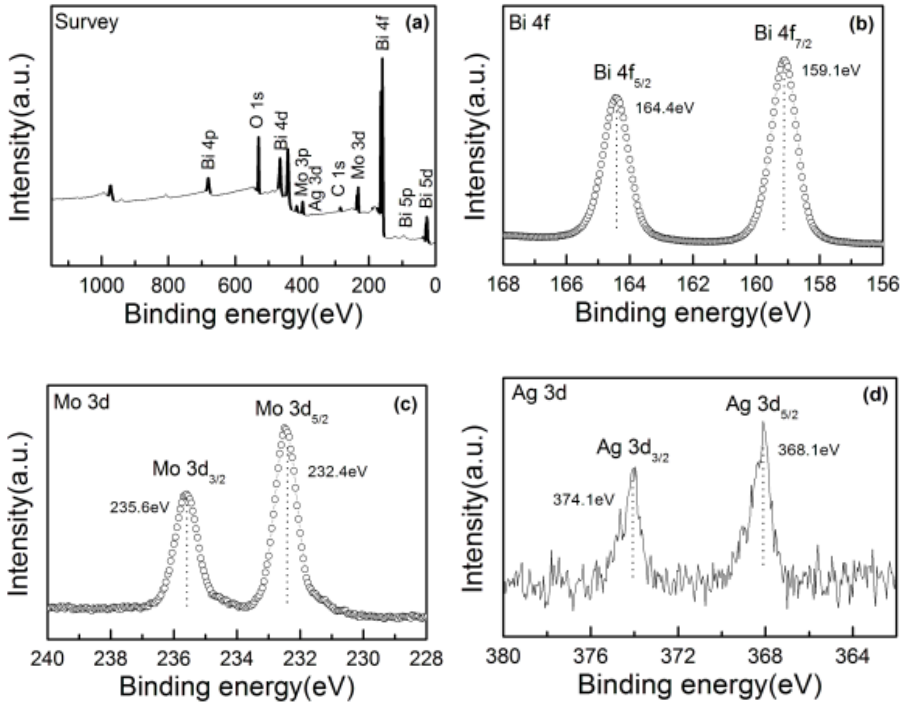

Fig. 3. XPS spectra of the as-prepared 7wt% Ag loaded Bi_2MoO_6 sample: (a) survey XPS spectrum, (b) Bi 4f, (c) Mo 3d, and (d) Ag.

3.2. Morphological Characterization

Figure 4 presents the SEM images for pure Bi_2MoO_6 (a), 3wt% Ag loaded Bi_2MoO_6 (b), 7wt% Ag loaded Bi_2MoO_6 (c), 11wt% Ag loaded Bi_2MoO_6 (d) sample. All of the samples displayed a flake-like morphology, and there were no differences in the macroscopic morphologies of the products. This suggested that a certain amount of Ag loading did not change the Bi_2MoO_6 morphology. Furthermore, the loaded Ag on the surface of the Bi_2MoO_6 nanoplates could not be identified. This is probably because the Ag particles might be too small to be detected. Thus, HRTEM was used to analyze the Ag/Bi_2MoO_6 composites, as shown in Figure 5.

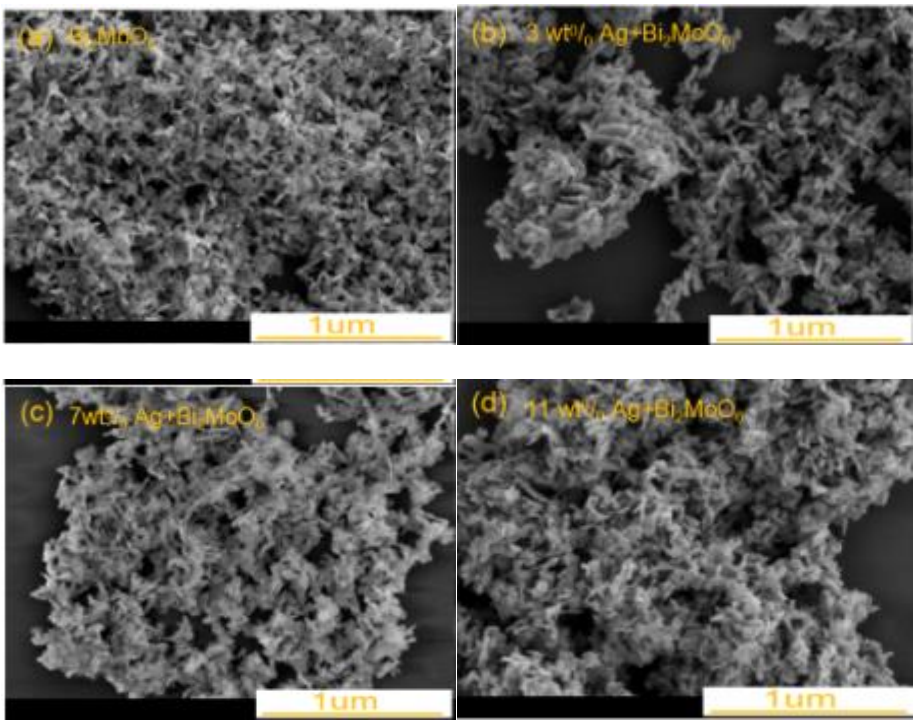

Fig. 4. SEM images of Ag/Bi_2MoO_6 nanosheets: (a) Bi_2MoO_6, (b) 3wt% Ag loaded Bi_2MoO_6, (c) 7wt% Ag loaded Bi_2MoO_6, and (d) 11wt% Ag loaded Bi_2MoO_6 (d).

Figure 5(a), (b) and (c) present the TEM images of pure Bi_2MoO_6, 5wt% and 7wt%Ag loaded Bi_2MoO_6 sample, respectively. For pure Bi_2MoO_6, thin and transparent nanoplates could be observed. Many black dots of Ag nanoparticles were observed which were uniformly distributed on the surface of the Bi_2MoO_6 nanoplates for 5wt% and 7wt%Ag loaded Bi_2MoO_6 samples. The average particle size for Ag nanoparticle was 2-4nm. Meanwhile, the HRTEM image for 7wt%Ag loaded Bi_2MoO_6 sample in Fig. 5(d) shows clear fringes with distances of 0.311nm and 0.231nm that correspond to (131) and (111) crystalline plane for Bi_2MoO_6 and Ag, respectively.

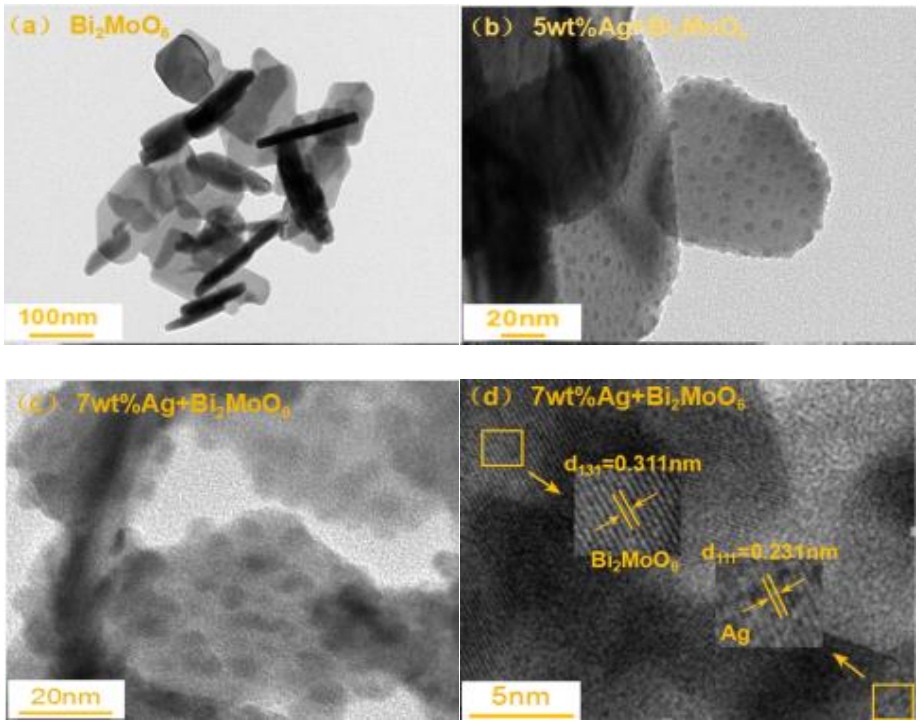

Fig. 5. TEM images of Ag/Bi_2MoO_6 nanosheets: (a) Bi_2MoO_6, (b) 5wt% Ag loaded Bi_2MoO_6, (c) 7wt% Ag loaded Bi_2MoO_6, and (d) HRTEM images of 7 wt%Ag loaded Bi_2MoO_6.

3.3. Optical Absorption Property of the Photocatalyst

For semiconductor materials, optical absorption property is one of important factors in determining the photocatalytic performance. The absorption spectra of the as-prepared Bi_2MoO_6 host and Ag-loaded Bi_2MoO_6 samples were recorded, and the results are presented in Figure 6. For Bi_2MoO_6, one strong absorption region appeared in the range of 200-400nm. This strong absorption region can be ascribed to intrinsic band gap transition, which resulted from electron transition from O 2p orbitals to Mo 4d orbitals.[24] Furthermore, a weak absorption band was observed around 480nm for samples with more than 5% Ag content. This band was most likely the SPR absorption of Ag-nanoparticles on the surface of Ag/Bi_2MoO_6 composites. In addition, all these absorption regions are from visible light region to UV light region. This suggested that the Bi_2MoO_6 samples might possibly show photocatalytic activities under visible light radiation. In general, Tauc approach is used to estimate photonic energy gap in crystalline semiconductors using the following equation $\alpha h\nu = A(h\nu - E_g)^{n/2}$, where α, h, ν, E_g and A are absorption coefficient, Planck constant, photon frequency, photonic energy gap and one constant, respectively.[25] The parameter n depends on the characteristics of the transitions in the semiconductor. For direct transitions, n=1, whereas for indirect transitions, n=4.[26] For n=1, the energy gap for the absorption edge can be determined by extrapolating the linear portion of the plot $(\alpha h\nu)^2$ vs $h\nu$ to zero absorbance. Correspondingly, the calculated energy gaps of 0 wt%, 1 wt%, 3 wt%, 5 wt%, 7 wt%, 9 wt%, and 11 wt% loaded Bi_2MoO_6 samples were 2.86, 2.78, 2.73, 2.72, 2.74, 2.43, and 2.69 eV, respectively, as shown in Figure 7. The results indicated that the band gap of the Ag/Bi_2MoO_6 nanocomposites become narrow in comparison with pure Bi_2MoO_6 due to the interaction between Ag and Bi_2MoO_6.

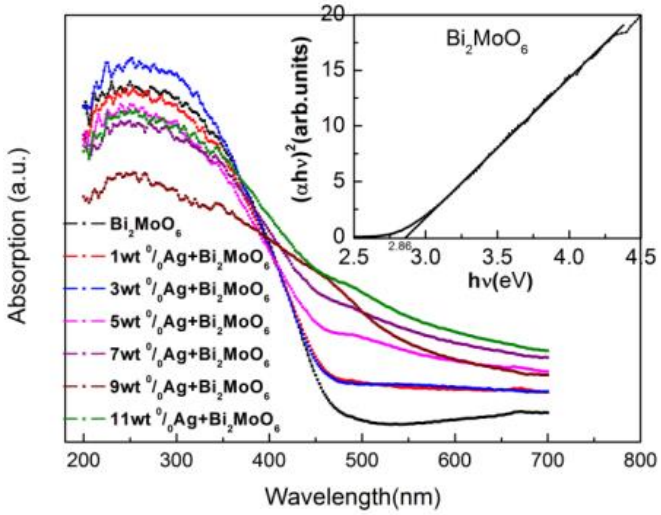

Fig. 6. UV-visible diffuse reflectance spectra for all samples; Inset: plots of $(\alpha h\nu)^2$ vs photo energy (hν) for pure Bi_2MoO_6 sample.

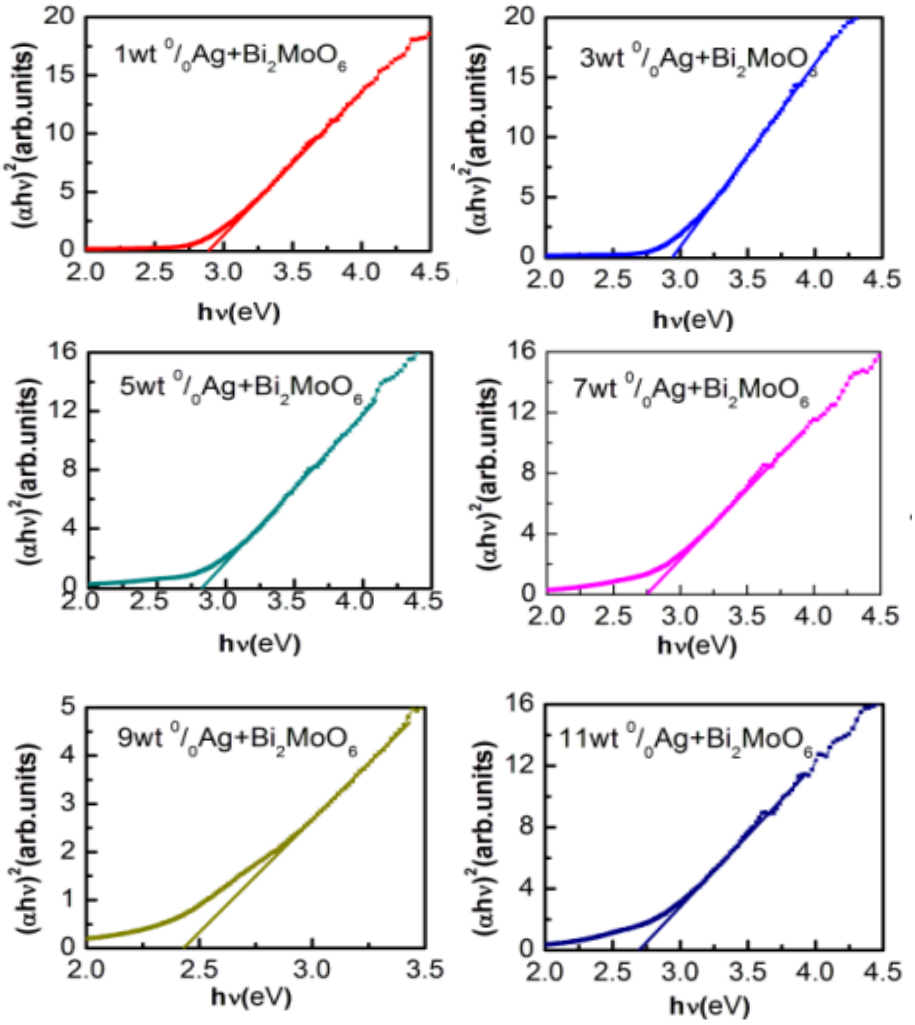

Fig. 7. The $(\alpha h\nu)^2$ vs photo energy (hν) curve for (a) 1wt%, (b) 3wt%, (c) 5wt%, (d) 7wt%, (e) 9wt%, (f) 11wt% Ag loaded Bi_2MoO_6 samples.

3.5. Photocatalytic Properties

The photocatalytic properties of Ag-loaded Bi_2MoO_6 samples were evaluated by the degradation efficiency of the RhB solvent. Before light irradiation, the dark absorption equilibrium between RhB molecules and the photocatalyst was achieved after stirring the suspension for 20min. Figure 8a presents the UV-vis absorption spectra for 9 wt%Ag loaded Bi_2MoO_6 sample at different light irradiation time. With increase in the irradiation time, the intensity of absorption decreased gradually. Moreover, when the irradiation time was increased to 120min, the absorption peak showed a blue shift from 554nm to 505nm.

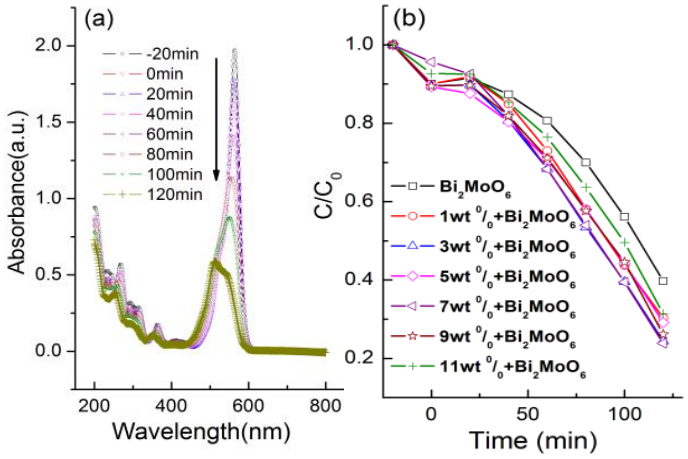

Fig. 8. (a) Absorption spectra of RhB with irradiation time with 9 wt% loaded Bi_2MoO_6, and (b) degradation rates of RhB under visible light irradiation the presence for all samples.

The corresponding photodegradation rates were also recorded and presented in Figure 8b. For pure Bi_2MoO_6, the degradation efficiency of RhB solution was about 62% within 120min. The degradation efficiency was found to improve under the same condition after loading the surface of Bi_2MoO_6 with Ag nanoparticles. The photocatalytic efficiency of 7 wt% Ag/Bi_2MoO_6 was enhanced to 77% within 120min. However, the photocatalytic efficiency of 11wt% Ag/Bi_2MoO_6 decreased to 69%. The photocatalytic efficiency for RhB was 62%, 70%, 74%, 71%, 77%, 74%, and 69% within 120 minutes for 0 wt%, 1 wt%, 3 wt%, 5 wt%, 7 wt%, 9 wt%, and 11 wt% Ag loaded Bi_2MoO_6 sample, respectively. Excess Ag nanoparticles may hinder the incoming visible light to irradiate on the Ag/Bi_2MoO_6 composites.[22,27] The enhancement of photocatalytic activity was observed due to the following two reasons. The SPR effect of Ag nanoparticles on the surface of the composites was a crucial reason for the efficient photodegradation of RhB. The SPR absorption peak of Ag nanoparticles is in the range of visible light, which led to strong absorption of the visible light. On the other hand, the heterojunction formation between Ag and Bi_2MoO_6 was another aspect, which increased the separation efficiency of the photoinduced electron-hole pairs and a lower recombination rate under visible light illumination.

In general, photocatalytic degradation of dyes is an oxidative process in which several active radical species may be involved, such as hole (h^+), superoxide anion radical ($\bullet O^{2-}$) and hydroxyl radicals (•OH). To evaluate the role of these active species, scavengers for h^+, $\bullet O^{2-}$ and •OH were added into 7 wt% Ag loaded Bi_2MoO_6 sample, and the corresponding results are shown in Figure 9. The scavengers used were isopropanol (IPA) for •OH, benzoquinone (BQ) for $\bullet O^{2-}$,

and oxaminic acid (OA) for h^+. The photocatalytic degradation rate of RhB over Ag/Bi_2MoO_6 under visible light showed minimal impact when IPA as a scavenger of •OH was added into the photoreaction system. By contrast, when BQ ($•O^{2-}$ scavenger) was added, the degradation rate of RhB was found to reduce, revealing that $•O^{2-}$ species were much more active than •OH in the photodegradation process. Furthermore, a large quenching effect was observed after the addition of OA (h^+ quencher), indicating that the holes played a dominant role in the RhB degradation. Thus, the photocatalytic activity was enhanced due to the effective inhibition of the recombination between electrons and holes.

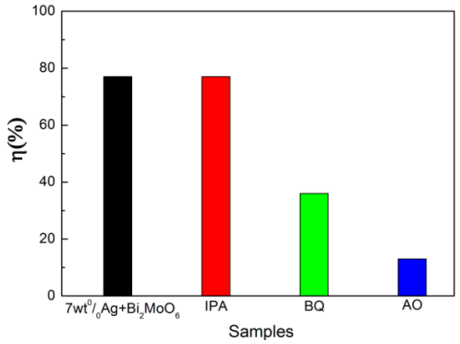

Fig. 9. Effects of different scavengers and corresponding degradation rate constant for the degradation of RhB with 7 wt% Ag/Bi_2MoO_6 composites.

Based on the above results, a possible photocatalytic mechanism for the superior photocatalytic performance of the ternary composite of Ag/Bi_2MoO_6 photocatalyst can be proposed by considering the charge transfer process (Fig. 10). In the system of Ag/Bi_2MoO_6, Bi_2MoO_6 can absorb visible-light photons to produce photogenerated electrons and holes. When the catalysts were illuminated, electrons in the valence band (VB) of Bi_2MoO_6 can be excited to the conduction band (CB) leaving back equal number of holes, as shown in Figure 9. Moreover, due to the SPR effect, photogenerated electron-hole pairs were also formed in the metallic Ag nanoparticles. The conduction band and valence band positions of the semiconductor at the point of zero charge can be calculated using the following formulas:

$$E_{VB}=\chi-E_e+0.5E_g$$

$$E_{CB}=\chi-E_e-0.5E_g$$

where E_{VB} is the potential of the valence band, χ is the electronegativity of the semiconductor which is the geometric mean of the electronegativity of the constituent atoms. The electronegativity value for Bi_2MoO_6 is 5.50eV.[28] E_e is the energy of free energy of free electrons on the hydrogen scale (4.5eV) and E_g is the band gap energy of the Bi_2MoO_6 semiconductor in Ag/Bi_2MoO_6 nanocomposite of value 2.86eV. The E_{VB} and E_{CB} were calculated to be 2.43 and -0.43eV, respectively.

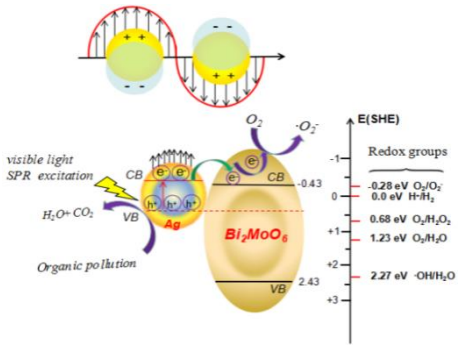

Fig. 10. Schematic illustration of the photocatalytic mechanism of Ag/Bi_2MoO_6 composites

Normally, a Schottky barrier is established when two materials with different work functions are combined with each other. In such a system, electrons move from the material with the low work function to the material with the high work function. In our samples, the Fermi energy of Ag is higher than that of Bi_2MoO_6, which led to transfer of electrons from the Fermi level of Ag to the Fermi level of Bi_2MoO_6, until the two levels reach equilibrium and form a new Fermi level, as shown in Figure 10. The electrons in the CB of Bi_2MoO_6 with strong reduction power can react with the absorbed O_2 to produce superoxide anion radicals ($\bullet O^{2-}$), which in turn oxidized RhB and resulted in a high photocatalytic degradation rate. Simultaneously, the VB holes remained on the Ag nanoparticles and Bi_2MoO_6 can react with H_2O/OH^- to generate hydroxyl radical species (•OH) with strong oxidizing power which can directly oxidize the dye molecule of RhB to CO_2, H_2O, and other molecules. This behavior reduced the recombination of photo-induced electrons and holes and prolonged the lifetime of the electron pairs. As a result, the photocatalytic activity increased due to Ag loading.

4. Conclusions

In summary, Ag/Bi_2MoO_6 composites photocatalyst was successfully synthesized via hydrothermal process and further used in the phorodegradation study of RhB. The structure, morphology, optical performance and crystallinity of the products were characterized by X-ray diffraction (XRD), field emission scanning electron microscope (FESEM) and (High resolution) transmission electron microscopy ((HR)TEM), and UV–visible diffuse reflectance spectroscopy (DRS), respectively.

The proposed mechanism can reasonably account for the high photocatalytic performance of Ag/Bi_2MoO_6 heterojunctions where electron-hole pair separation could be maintained very efficiently. The surface plasmon resonance of Ag/Bi_2MoO_6 was a major reason for the high photocatalytic performance of organic pollutants degradation. At the same time, the synergistic effect of Ag and Bi_2MoO_6 could generate more heterojunctions which promoted photoelectrons transfer from Ag to Bi_2MoO_6, leading to an improvement in the photocatalytic performance through suppression of photoelectrons-holes recombination. Finally, the 7wt% Ag-loaded Bi_2MoO_6 showed the optimal photocatalytic performance in the photodegradation of RhB.

Acknowledgments

This work was financially supported by National first class curriculum (Physical properties of materials). Open fund for Discipline Construction,Institutes of Physical Science and Information Technology, Anhui University. National Training Programs of Innovation and Entrepreneurship for Undergraduates (202010357021, 202010357296). Anhui Province Key Laboratory of Chemistry for Inorganic/Organic Hybrid Functionalized Materials, Anhui University,Anhui Provincial Natural Science Foundation (1308085MA04), and the Higher Educational Natural Science Foundation of Anhui Province (KJ2013A031).

References

[1] N. Zhang, R. Ciriminna, M. Pagliaro, Y. J. Xu, Chem. Soc. Rev. 43, 5276 (2014); https://doi.org/10.1039/C4CS00056K

[2] J. Zhang, C. G. Niu, J. Ke, L. F. Zhou, G. M. Zeng, Catal. Commun. 59, 30 (2015); https://doi.org/10.1016/j.catcom.2014.09.041

[3] Y. N. Zhu, J. J. Mu, G. H. Zheng, Z. X. Dai, L. Y. Zhang, Y. Q. Ma, D. W. Zhang, Ceram. Int. 42, 17347 (2016); https://doi.org/10.1016/j.ceramint.2016.08.031

[4] W. Z. Wang, W. W. Zhang, S. Meng, L. J. Jia, M. Tan, C. C. Hao, Y. J. Liang, J. Wang, B. Zou, Electron. Mater. Lett. 12, 753 (2016); https://doi.org/10.1007/s13391-016-6224-9

[5] K. Cho, M. R. Hoffmann, Appl. Catal B Environ. 202, 671 (2017); https://doi.org/10.1016/j.apcatb.2016.09.067

[6] Y. Shimodaira, H. Kato, H. Kobayashi, A. Kudo, J. Phys. Chem. C. 110, 17790 (2006); https://doi.org/10.1021/jp0622482

[7] S. C. Zhang, C. Zhang, Y. Man, Y. F. Zhu, J. Solid State Chem. 179, 62 (2006); https://doi.org/10.1016/j.jssc.2005.09.041

[8] J. Ke, X. G. Duan, S. Luo, H. Y. Zhang, H. Q. Sun, J. Liu, M. Tode, S. B. Wang, Chem. Eng. J 313, 1447 (2017); https://doi.org/10.1016/j.cej.2016.11.048

[9] A. A. Alemi, R. Kashfi, B. Shabani, J. Mol. Catal A Chem. 392, 290 (2014); https://doi.org/10.1016/j.molcata.2014.05.029

[10] L. W. Zhang, T. G. Xu, X. Zhao, Y. F. Zhu, Appl. Catal B Environ. 98, 138 (2010); https://doi.org/10.1016/j.apcatb.2010.05.022

[11] S. Y. Lee, J. Kim, B. Ahn, I. S. Cho, H. K. Yu, H. Seo, Electron. Mater. Lett. 13, 107 (2017); https://doi.org/10.1007/s13391-017-6384-2

[12] S. V. P. Vattikuti, C. Byon, C. V. Reddy, Electron. Mater. Lett. 12, 812 (2016); https://doi.org/10.1007/s13391-016-6267-y

[13] P. Christopher, H. Xin, S. Linic, Nat. Chem. 3, 467 (2011); https://doi.org/10.1038/nchem.1032

[14] S. Linic, U. Alsam, C. Boerigter, M. Morabitio, Nat. Mater. 14, 567 (2015); https://doi.org/10.1038/nmat4281

[15] B. Zhou, X. Zhao, H. J. Liu, J. H. Qu, C. P. Huang, Sep. Purif. Techno. 77, 275 (2011);

https://doi.org/10.1016/j.seppur.2010.12.017

[16] M. G. Wang, W. Lu, D. Chen, J. Liu, X. Hu, L. Jin, Y. S. Lin, D. Yue, J. B. Huang, Z. L. Wang, Mater. Res. Bull. 84, 414 (2016); https://doi.org/10.1016/j.materresbull.2016.08.043

[17] S. Bai, J. Jiang, Q. Zhang, Y. J. Xiong, Chem. Sov. Rev. 44, 2893 (2015); https://doi.org/10.1039/C5CS00064E

[18] H. S. Jung, H. Kim, Electron. Mater. Lett. 5, 73 (2009); https://doi.org/10.3365/eml.2009.06.073

[19] J. P. Yang, F. Zhang, Y. R. Chen, S. Qian, P. Hu, W. Li, Y. H. Deng, Y. Fangm, M. Luqman, D. Y. Zhao, Chem. Commun. 47, 11618 (2011); https://doi.org/10.1039/c1cc15304h

[20] K. T. Ranjit, I. Willner, S. H. Bossmann, A. M. Braun, J.Catal. 204, 305 (2001); https://doi.org/10.1006/jcat.2001.3388

[21] K. T. Ranjit, I. Willner, S. H. Bossmann, A. M. Braun, Environ. Sci. Technol. 35, 1544 (2001); https://doi.org/10.1021/es001613e

[22] A. Phuruangrat, S. Putdum, P. Dumrongrojthanath, N. Ekthammathat, S. Thongtem, T. Thongtem, Mat. Sci. Semicon. Proc. 34, 175 (2015); https://doi.org/10.1016/j.mssp.2015.02.028

[23] Y. Y. Luo, G. Q. Tan, G. H. Dong, L. L. Zhang, J. Huang, W. Yang, C. C. Zhao, H. J. Ren, Appl. Surf. Sci. 324, 505 (2015); https://doi.org/10.1016/j.apsusc.2014.10.168

[24] Y. Shimodaira, H. Kato, H. Kobayashi, A. Kudo, J. Phys. Chem B 110, 17790 (2006); https://doi.org/10.1021/jp0622482

[25] M. Butler, J. Appl. Phys. 48, 1914 (1997); https://doi.org/10.2307/591153

[26] X. Zhang, Z. Ai, F. Jia, L. Zhang, X. Fan, B. Z. Zou, Mater. Chem. Phys. 103, 162 (2007); https://doi.org/10.1016/j.matchemphys.2007.02.008

[27] A. Phuruangrat, S. Putdum, P. Dumrongrojthanath, N. Ekthammathat, S. Thongtem, T. Thongtem, E. Hong, D. Kim, J. H. Kim, J. Ind. Eng. Chem. 20, 3869 (2014); https://doi.org/10.1155/2014/138561

[28] J. L. Zhang, L. S. Zhang, N. Yu, K. B. Xu, S. J. Li, H. L. Wang, J. S. Liu, RCS advances 5, 75081 (2015); https://doi.org/10.1039/C5RA13148K